# Spin-wave resonances in bismuth orthoferrite at high temperatures

M. Białek,[1,*] A. Magrez,[1] A. Murk,[2] and J.-Ph. Ansermet[1]
[1]*Institute of Physics, École Polytechnique Fédérale de Lausanne (EPFL), 1015 Lausanne, Switzerland*
[2]*Institute of Applied Physics, University of Bern, Silderstrasse 5, 3012 Bern, Switzerland*

(Received 30 October 2017; revised manuscript received 11 January 2018; published 12 February 2018)

Spin-wave resonances in pelletized powder of bismuth orthoferrite ($BiFeO_3$) were studied in transmission spectroscopy at frequencies of 0.1–0.75 THz and in the temperature range of 300–650 K. A vector network analyzer with frequency extenders was used in conjunction with temperature scans. We extended the experimental coverage of spin-wave resonances in $BiFeO_3$ up to almost the Néel temperature. We observed that $\Psi_1^{(1)}$ and $\Psi_1^{(2)}$ modes are degenerate around 420 K due to the temperature dependences of the magnetic anisotropy and the Dzyaloshinskii-Moriya interaction.

DOI: 10.1103/PhysRevB.97.054410

## I. INTRODUCTION

Bismuth orthoferrite $BiFeO_3$ (BFO) has been studied intensively over the past few years because it promises multiple possible uses, including spintronic devices or memristors [1]. It is a room-temperature multiferroic, showing simultaneously magnetic and ferroelectric orders [2]. Bismuth ferrite crystallizes in the rhombohedrally distorted perovskite structure in the space group $R3c$. The Néel temperature of bismuth ferrite is 643 K, and the ferroelectric Curie temperature is about 1100 K [3]. There are reports showing magnetoelectric coupling in BFO [4–7]. Iron atoms form a monoclinic lattice with spins in $G$-type antiferromagnetic order [8]. To a first approximation, spins are oriented ferromagnetically within hexagonal layers and antiferromagnetically between adjacent layers. What differentiates BFO from most of the other rare-earth orthoferrites is that its magnetic order is periodic—the antiferromagnetic axis is rotating with an incommensurate period of 62 nm [9]. This static structure, known as the spin cycloid, results from the Dzyaloshinskii-Moriya (DM) interaction [10]. The wave vector of the spin cycloid has three possible directions within a hexagonal layer of Fe atoms. The rotation plane of the spin cycloid is defined by its wave vector and the direction of the electrical polarization ([1,1,1] in the pseudocubic notation). As the spins are locally canted [11], there is a local ferromagnetic moment that has the same period of 62 nm. Bismuth ferrite spin structure might be changed to a nonperiodic, weakly ferromagnetic state, either by applying high magnetic fields [12], high pressure [13], or strain [14].

The existence of a periodic spin structure allows for an optical excitation of multiple modes of spin waves. A thermodynamic model was developed by de Sousa *et al.*, which describes these modes as wavelike distortions of the spin cycloid [15]. A quantum-mechanical model of magnons in BFO has been developed by Fishman *et al.* [16–18]. The Hamiltonian, describing spin-wave modes in BFO, contains five parameters: $J_1$, nearest-neighbor exchange interaction; $J_2$, next-nearest-neighbor exchange interaction; $K$, anisotropy; $D_1$, DM interaction between atoms within a hexagonal iron plane; and $D_2$, DM interaction between atoms in adjacent hexagonal layers. Two families of magnon modes can be excited: $\Phi$ waves with spins oscillating in the plane of the cycloid, and $\Psi$ waves with an oscillation out of the plane of the cycloid. The dispersion relation of $\Psi$ modes is $\sim\sqrt{1+k^2}$, while that of $\Phi$ is $\sim|k|$. The spin cycloid wave vector $2\pi/62$ nm$^{-1}$ is small enough for frequencies of $\Phi$ and $\Psi$ magnon modes in BFO to be distinct. Additionally, modes are split due to the presence of higher harmonics of the spin cycloid caused by the anisotropy and $D_2$ interaction [17]. There is an ongoing debate on the amplitude of the anharmonicity of the spin cycloid in $BiFeO_3$ [19–21]. The investigation of spin-wave modes presented in this paper is sustained by the theoretical model from Refs. [16–18].

Magnon modes in $BiFeO_3$ were under investigation in recent years using either inelastic neutron scattering [11,14,22,23], Raman scattering spectroscopy [7,13,24–26], THz time-domain spectroscopy [27], or far-infrared Fourier spectroscopy [28,29]. Most of these studies focused on phenomena at low temperatures, even though BFO shows multiferroic behavior up to almost 400 °C. Our experimental system provides us with stability, high dynamic range, and high spectral resolution, which allows us to characterize these spin-wave resonances at high temperatures.

## II. EXPERIMENT

The sample preparation process was explained in Ref. [30]. X-ray diffractometry measurements confirmed samples to be rhombohedral BFO without detectable parasitic inclusions. X-ray fluorescence spectroscopy confirmed that our samples are stoichiometric with 0.3% uncertainty. This $BiFeO_3$ powder was pressed into ceramic pellets of about $12 \times 12 \times 2$ mm$^3$, then cut into smaller pieces of about $7 \times 5 \times 2$ mm$^3$.

*marcin.bialek@epfl.ch

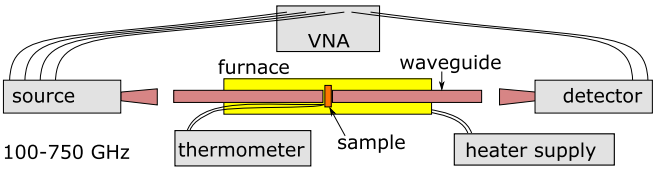


FIG. 1. Scheme of the experimental setup.

The experimental setup uses a vector network analyzer (VNA) and Virginia Diodes (VDI) frequency extenders. In the current setup it was possible to cover three bands, 100–175, 200–350, and 470–750 GHz.[1] A similar setup was used in the investigation of resonances at low temperatures [30]. We also performed measurements at the University of Bern with 345–415 and 415–470 GHz bands to cover the intermediate frequency region. The VNA with frequency extenders measures the amplitude and phase of the electric field of the incoming radiation. We measured transmission, which was affected mostly by the absorption in the case of investigated samples. We report on a logarithmic scale the amplitude of the $S_{21}$ signal normalized to the source output. The schematic of the experimental setup is presented in Fig. 1. The sample was placed in a cylindrical ceramic furnace 20 cm in length mounted on an optical bench. Terahertz radiation was guided to the sample using oversized metallic waveguides of 6 mm diamater and 20 cm length. The source and detector mixers were coupled to the waveguide using corrugated horn antennas. The high-temperature part of the setup was separated from the mixers by Teflon windows. The sample was mounted in the middle of the furnace.

During the measurement, the power supplied to the furnace heater wire was slowly increased producing a temperature ramp. The temperature was measured using a $K$-type thermocouple placed close to the sample. A typical run from room temperature to 400 °C took 2–3 h. During the time taken to measure one spectrum, the temperature of the sample was changing by less than 1.0 K.

Figure 2(a) shows an exemplary result obtained at $T = 445$ K. Such data hardly show any resonances due to multiple interferences that strongly modulate the spectra as a function of $f$ but independent of sample temperature. To overcome this issue, data must be analyzed to reveal temperature dependencies. This was done by calculation of temperature-differential transmission spectra:

$$\frac{\partial S_{21}}{\partial T}(f,T) = \frac{S_{21}(f,T+\Delta T) - S_{21}(f,T)}{\Delta T}. \qquad (1)$$

To simplify this process, $S_{21}(f,T)$ were interpolated as a function of temperature $T$ with a step $\Delta T$. This step was chosen to be of the order of the mean temperature step between measured spectra, i.e., in the case of data presented in Fig. 2(b), $\Delta T$ was 1.0 K. Calculation of temperature derivative spectra reveals only phenomena that depend on temperature. Since frequencies of magnetic resonances in BFO are expected to go to zero when approaching the Néel temperature, this method of data treatment is expected to produce clear results at temperatures above 300 K.

[1]We drove the VNA system a little out of the ranges specified by the manufacturer. We found that the signal was stable enough for our purpose, 10–20 GHz out of the designed range.

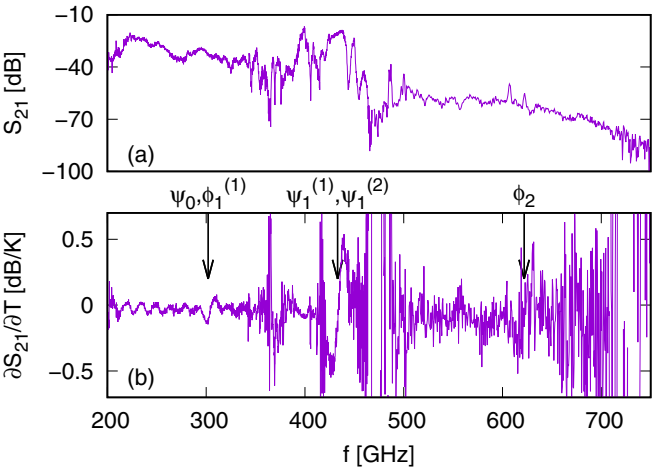


FIG. 2. Example of analysis of data obtained at temperature $T = 445$ K. (a) Spectrum of transmission magnitude $S_{21}$, (b) spectrum of temperature derivative of $S_{21}$. Identification of modes is in Sec. III.

## III. RESULTS

Temperature-differential transmission results are presented in Fig. 3. Such a presentation of subsequent differential spectra allows us to distinguish four resonant lines superimposed over a temperature-dependent interference. The interference is due to a dependence of the sample dielectric constant on temperature. The identification of modes, as presented in the following paragraphs, is based on their frequencies at room temperature as compared with other experimental data [27,31,32].

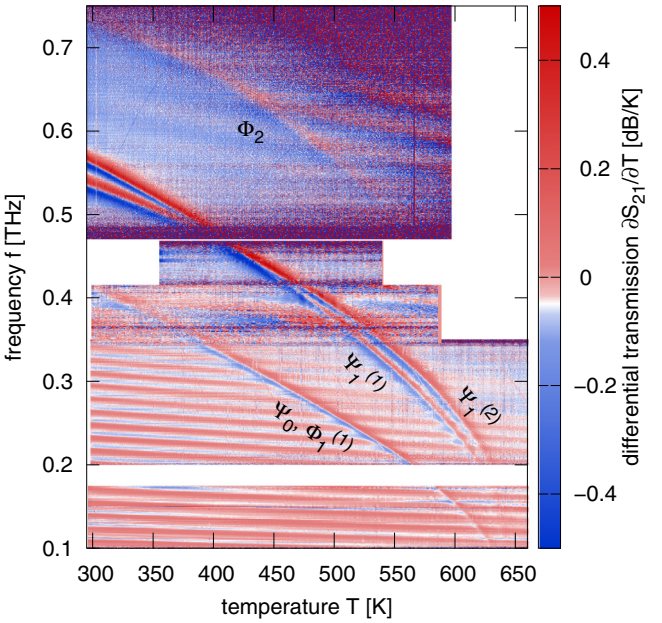


FIG. 3. Temperature-differential transmission in bismuth ferrite as a function of frequency and temperature.

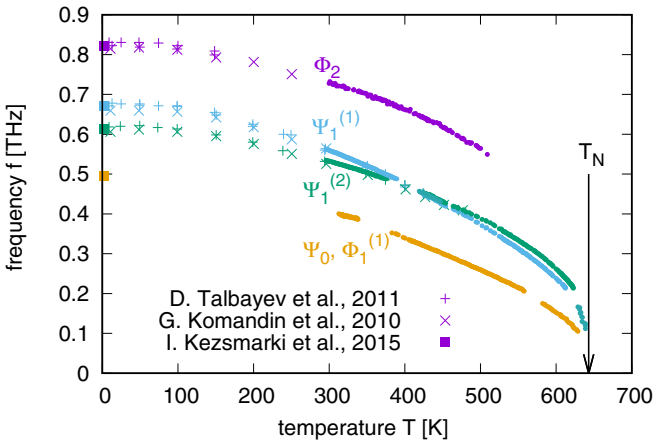


FIG. 4. Frequencies of observed resonant features as a function of sample temperature (small dots). Points of different shapes represent data imported from D. Talbayev *et al.* (Ref. [27]), G. Komandin *et al.* (Ref. [31]), and I. Kézsmárki *et al.* (Ref. [32]).

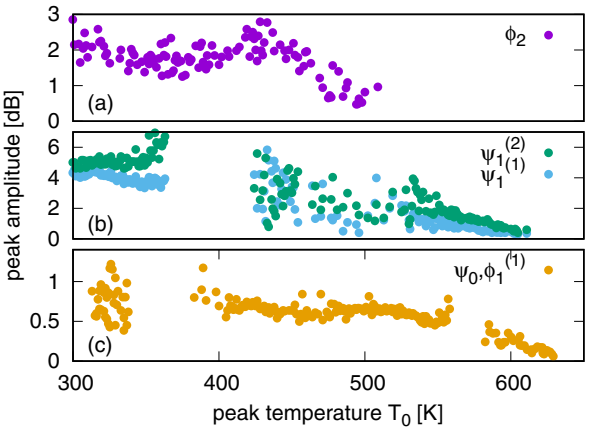


FIG. 5. Amplitudes of observed resonances as a function of resonance temperature $T_0$: (a) for $\Phi_2$ mode, (b) for $\Psi_1^{(1)}$ and $\Psi_1^{(2)}$ modes, and (c) for degenerated $\Psi_0$ and $\Phi_1^{(1)}$ modes.

To obtain quantitative results from these data, we fitted a simple model describing the differential signal. We assumed that resonance is a derivative of the Lorentzian distribution superimposed over a phenomenological function describing an oscillatory background. Fits were performed for fixed temperatures $\frac{\partial S_{21}}{\partial T}(f, T_0)$ as a function of frequency. In the case of data in the 100–175 GHz band, fits were performed as a function of temperature, because resonant features were very weak. Such a procedure allowed for their examination over a smoother background, with the cost of a loss of accuracy in determining amplitudes and widths. A similar procedure was used at around 490 and 200 GHz to obtain resonance positions, when fits in the frequency direction failed due to a partial coverage of features.

Two strong resonant features, visible at room temperature at 500–600 GHz (Fig. 4), are $\Psi_1^{(2)}$ and $\Psi_1^{(1)}$ modes. They appear to intersect at $T = 422 \pm 2$ K, $f = 456.4 \pm 1.6$ GHz. The question arises as to the identification of these modes above this temperature. To answer it, we analyzed the amplitudes and widths of these resonances. The low-frequency mode has greater amplitude in the $f \geqslant 470$ GHz, $T_0 \leqslant 410$ K region, whereas in the $f \leqslant 470$ GHz, $T_0 \geqslant 410$ K region the high-frequency mode amplitude is larger [Fig. 5(b)]. The widths of both resonances are similar above 420 K [Fig. 6(b)]. Thus we concluded that $\Psi_1^{(2)}$ and $\Psi_1^{(1)}$ modes have crossed at $T = 422$ K.

The amplitudes of $\Psi_1^{(2)}$ and $\Psi_1^{(1)}$ modes start dropping at around 400 K [Fig. 5(b)], which is in the frequency range not covered by our results (Fig. 3). In the case of results in the 100–175 GHz band (above 625 K), only a single weak resonance was observed. It is unknown whether this resonance is $\Psi_1^{(2)}$, $\Psi_1^{(1)}$, or both being convoluted. Therefore, for these temperatures, only results regarding the position of this single feature are presented (Fig. 4).

The lowest frequency mode is identified as degenerate $\Phi_1^{(1)}$ and $\Psi_0$ modes (Fig. 4). Although there are no experimental data for this mode above 5 K, this is the only optically active mode below $\Psi_1$ modes. The amplitude of this resonance is roughly constant until ≈510 K, above which it starts dropping [Fig. 5(c)]. The width [Fig. 6(c)] shows a broad minimum centered around 500 K. The oscillation of the width is an artifact due to its shift relative to the interference pattern [Fig. 3].

The mode with a frequency of 730 GHz at room temperature is $\Phi_2$ (Fig. 4). Experimentally, this is the most difficult resonance to detect since it is observed with low transmitted powers and it is broader than other modes [Fig. 6(a)] while it has quite a low amplitude [Fig. 5(a)]. Note that the amplitude of the $\Phi_2$ mode shows a maximum at $T \approx 425$ K, which coincides with the temperature at which $\Psi_1$ modes intersect.

## IV. DISCUSSION

The disappearance of the $\Psi_1$ mode splitting indicates that around 422 K the spin cycloid passes through a point of higher symmetry. Following Ref. [17], the magnetic anisotropy $K$ and DM interaction $D_2$ generate higher-order harmonics of the spin cycloid. Thus, both split the frequencies of spin-wave modes. Therefore, the crossing of $\Psi_1$ modes results from anisotropy and $D_2$ interaction canceling each other's effects

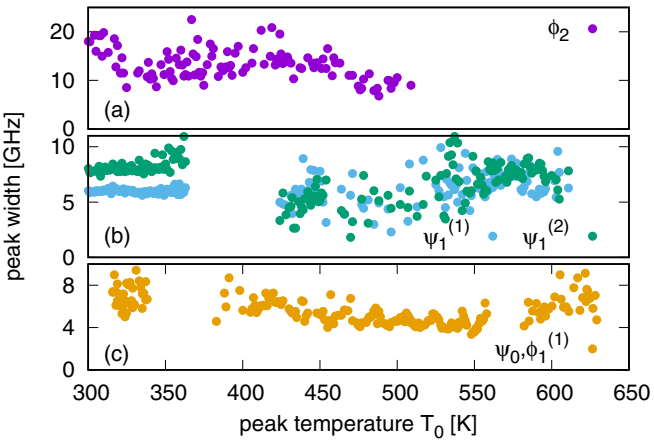


FIG. 6. Widths of observed resonant features as a function of resonance temperature $T_0$: (a) for $\Phi_2$ mode, (b) for $\Psi_1^{(1)}$ and $\Psi_1^{(2)}$ modes, and (c) for degenerated $\Psi_0$ and $\Phi_1^{(1)}$ modes.

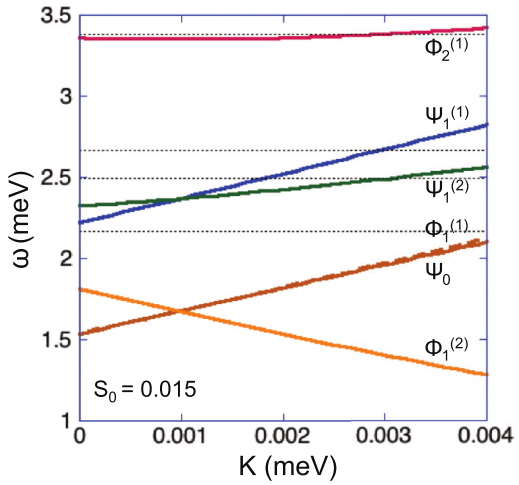


FIG. 7. Dependence of frequencies of spin-wave modes in BFO on anisotropy $K$, with the DM interaction parameter $D_2 = 54$ $\mu$eV. Figure imported from Ref. [17].

on the frequencies of the spin-wave modes (Fig. 7). As long as the spin cycloid has no higher harmonics at this temperature, it is in a canted state and its symmetry is lower than in an ideal situation for $K = D_2 = 0$. The splitting reflects the presence of a band gap in a magnon band structure at the spin cycloid wave vector [17]. Thus, around 422 K the band gap is closed and the band structure has two spin-wave branches of nearly linear dispersions.

The temperature at which $\Psi_1$ modes cross is weakly reflected in the behaviors of two other observed modes. The $\Phi_1^{(2)}$ mode is optically inactive, and indeed it is not observed in our results. It should cross with $\Phi_1^{(1)}$ at the same value of anisotropy as $\Psi_1$ modes do (Fig. 7) [17], but no disturbance of $\Phi_1^{(1)}$ at this temperature is observed [Figs. 5(c) and 6(c)]. On the other hand, the $\Phi_2$ mode amplitude increases at the temperature corresponding to the intersection of $\Psi_1^{(1)}$ and $\Psi_1^{(2)}$ modes [Fig. 5(a)]. There are reports of a dielectric anomaly in BFO appearing at $T_P \approx 460$ K, referred to as the Połomska transition [3,33–36]. The proximity of the observed crossing suggests that the Połomska transition might be related to magnetism, as suggested in Ref. [3], and that it is connected with a change of the magnetic anisotropy.

The dependence of mode frequencies on temperature sharpens slowly when approaching $T_N$. For example, $\Phi_1^{(1)}$ and $\Psi_0$ modes at 99% of $T_N$ have still ≈21% of their frequencies at $T = 0$ K. This value does not contradict with the strength of the internal magnetic fields in rare-earth orthoferrites as determined by Mössbauer spectroscopy within the experimental uncertainty [37]. Considering widths of resonances, an almost vertical frequency-temperature dependence is expected at frequencies below 100 GHz. As amplitudes drop very fast when approaching the Néel temperature, an observation of magnon modes so close to it becomes a very demanding experimental task.

## V. CONCLUSIONS

We have characterized spin-wave resonances in bismuth ferrite at high temperatures using a vector network analyzer with frequency extenders. We detected resonances by determining the temperature derivative of the transmission. Our results extend the investigation of excitations of the spin cycloid to low frequencies and high temperatures by approaching the Néel temperature. We show that two of the spin-wave resonances in BFO are degenerate at $T = 422$ K, which is explained as the result of the dependence of the spin cycloid anharmonicity on temperature.

## ACKNOWLEDGMENTS

Work partially supported by a Requip (206021 150707/1) grant of the Swiss National Science Foundation and by EPFL.

[1] M. Bibes, A. Barthelemy, J. Grollier, and J. Mage, Ferroelectric device with adjustable resistance, WO 2010142762 A1 (2010).
[2] D. Lebeugle, D. Colson, A. Forget, M. Viret, P. Bonville, J. F. Marucco, and S. Fusil, Phys. Rev. B **76**, 024116 (2007).
[3] G. Catalan and J. F. Scott, Adv. Mater. **21**, 2463 (2009).
[4] C. Tabares-Muñoz, J.-P. Rivera, A. Bezinges, A. Monnier, and H. Schmid, Jpn. J. Appl. Phys. **24**, 1051 (1985).
[5] T. Zhao, A. Scholl, F. Zavaliche, K. Lee, M. Barry, A. Doran, M. P. Cruz, Y. H. Chu, C. Ederer, N. A. Spaldin, R. R. Das, D. M. Kim, S. H. Baek, C. B. Eom, and R. Ramesh, Nat. Mater. **5**, 823 (2006).
[6] Y.-H. Chu, L. W. Martin, M. B. Holcomb, M. Gajek, S.-J. Han, Q. He, N. Balke, C.-H. Yang, D. Lee, W. Hu, Q. Zhan, P.-L. Yang, A. Fraile-Rodriguez, A. Scholl, S. X. Wang, and R. Ramesh, Nat. Mater. **7**, 478 (2008).
[7] P. Rovillain, R. de Sousa, Y. Gallais, A. Sacuto, M. A. Méasson, D. Colson, A. Forget, M. Bibes, A. Barthélémy, and M. Cazayous, Nat. Mater. **9**, 975 (2010).
[8] C. Ederer and N. A. Spaldin, Phys. Rev. B **71**, 060401(R) (2005).
[9] I. Sosnowska, T. P. Neumaier, and E. Steichele, J. Phys. C **15**, 4835 (1982).
[10] I. Sosnowska and A. K. Zvezdin, J. Magn. Magn. Mater. **140**, 167 (1995).
[11] M. Ramazanoglu, M. Laver, W. Ratcliff, S. M. Watson, W. C. Chen, A. Jackson, K. Kothapalli, S. Lee, S.-W. Cheong, and V. Kiryukhin, Phys. Rev. Lett. **107**, 207206 (2011).
[12] B. Ruette, S. Zvyagin, A. P. Pyatakov, A. Bush, J. F. Li, V. I. Belotelov, A. K. Zvezdin, and D. Viehland, Phys. Rev. B **69**, 064114 (2004).
[13] J. Buhot, C. Toulouse, Y. Gallais, A. Sacuto, R. de Sousa, D. Wang, L. Bellaiche, M. Bibes, A. Barthélémy, A. Forget, D. Colson, M. Cazayous, and M.-A. Measson, Phys. Rev. Lett. **115**, 267204 (2015).
[14] D. Sando, A. Agbelele, D. Rahmedov, J. Liu, P. Rovillain, C. Toulouse, I. C. Infante, A. P. Pyatakov, S. Fusil, E. Jacquet, C. Carrétéro, C. Deranlot, S. Lisenkov, D. Wang, J.-M. Le Breton, M. Cazayous, A. Sacuto, J. Juraszek, A. K. Zvezdin,

L. Bellaiche, B. Dkhil, A. Barthélémy, and M. Bibes, Nat. Mater. **12**, 641 (2013).
[15] R. de Sousa and J. E. Moore, Phys. Rev. B **77**, 012406 (2008).
[16] R. S. Fishman, N. Furukawa, J. T. Haraldsen, M. Matsuda, and S. Miyahara, Phys. Rev. B **86**, 220402 (2012).
[17] R. S. Fishman, J. T. Haraldsen, N. Furukawa, and S. Miyahara, Phys. Rev. B **87**, 134416 (2013).
[18] R. S. Fishman, J. H. Lee, S. Bordács, I. Kézsmárki, U. Nagel, and T. Rõõm, Phys. Rev. B **92**, 094422 (2015).
[19] A. V. Zalesskii, A. A. Frolov, A. K. Zvezdin, A. A. Gippius, E. N. Morozova, D. F. Khozeevc, A. S. Bush, and V. S. Pokatilov, J. Exp. Theor. Phys. **95**, 101 (2002).
[20] I. Sosnowska and R. Przeniosło, Phys. Rev. B **84**, 144404 (2011).
[21] D. Rahmedov, D. Wang, J. Íñiguez, and L. Bellaiche, Phys. Rev. Lett. **109**, 037207 (2012).
[22] M. Matsuda, R. S. Fishman, T. Hong, C. H. Lee, T. Ushiyama, Y. Yanagisawa, Y. Tomioka, and T. Ito, Phys. Rev. Lett. **109**, 067205 (2012).
[23] J. Jeong, M. D. Le, P. Bourges, S. Petit, S. Furukawa, S.-A. Kim, S. Lee, S.-W. Cheong, and J.-G. Park, Phys. Rev. Lett. **113**, 107202 (2014).
[24] M. Cazayous, Y. Gallais, A. Sacuto, R. de Sousa, D. Lebeugle, and D. Colson, Phys. Rev. Lett. **101**, 037601 (2008).
[25] M. K. Singh, R. S. Katiyar, and J. F. Scott, J. Phys.: Condens. Matter **20**, 252203 (2008).
[26] A. Kumar, J. F. Scott, and R. S. Katiyar, Appl. Phys. Lett. **99**, 062504 (2011).
[27] D. Talbayev, S. A. Trugman, S. Lee, H. T. Yi, S.-W. Cheong, and A. J. Taylor, Phys. Rev. B **83**, 094403 (2011).
[28] U. Nagel, R. S. Fishman, T. Katuwal, H. Engelkamp, D. Talbayev, H. T. Yi, S.-W. Cheong, and T. Rõõm, Phys. Rev. Lett. **110**, 257201 (2013).
[29] S. Skiadopoulou, V. Goian, C. Kadlec, F. Kadlec, X. F. Bai, I. C. Infante, B. Dkhil, C. Adamo, D. G. Schlom, and S. Kamba, Phys. Rev. B **91**, 174108 (2015).
[30] C. Caspers, V. P. Gandhi, A. Magrez, E. de Rijk, and J.-P. Ansermet, Appl. Phys. Lett. **108**, 241109 (2016).
[31] G. A. Komandin, V. I. Torgashev, A. A. Volkov, O. E. Porodinkov, I. E. Spektor, and A. A. Bush, Phys. Solid State **52**, 734 (2010).
[32] I. Kézsmárki, U. Nagel, S. Bordács, R. S. Fishman, J. H. Lee, H. T. Yi, S.-W. Cheong, and T. Rõõm, Phys. Rev. Lett. **115**, 127203 (2015).
[33] M. Połomska, W. Kaczmarek, and Z. Pająk, Phys. Status Solidi A **23**, 567 (1974).
[34] P. Fischer, M. Połomska, I. Sosnowska, and M. Szymański, J. Phys. C **13**, 1931 (1980).
[35] A. Kumar, J. F. Scott, and R. S. Katiyar, Phys. Rev. B **85**, 224410 (2012).
[36] P. K. Jha, P. A. Jha, V. Singh, P. Kumar, K. Asokan, and R. K. Dwivedi, J. Appl. Phys. **117**, 024102 (2015).
[37] M. Eibschütz, S. Shtrikman, and D. Treves, Solid State Commun. **4**, 141 (1966).